Realizing the Resolution Enhancement of Tube-to-Tube Plate Friction Welding Microstructure Images Via Hybrid Sparsity Model for Improved Weld Interface Defects Diagnosis

Kathiravan Srinivasan[1], N Deepa[1], Durai Raj Vincent P M[1], Senthil Kumaran S[2]

[1] School of Information Technology and Engineering, Vellore Institute of Technology (VIT), Vellore, India
[2] School of Mechanical Engineering, Vellore Institute of Technology (VIT), Vellore, India
kathiravan.srinivasan@vit.ac.in, deepa.rajesh@vit.ac.in, pmvincent@vit.ac.in, senthilkumaran.s@vit.ac.in

Abstract

Weld interface defects at a one-micrometer level can be identified with the support of the optical microscope (OM) images. However, identification of such defects below one-micrometer becomes challenging due to the limited resolution of OM imaging. Besides, the diagnosis gets even more challenging when the OM equipment is in worn-out condition. This research develops a hybrid sparsity model for efficiently improving the resolution of the degraded weld microstructure images. Rather than using a colossal patch databank for training, we deploy two condensed well-learned dictionaries. The sparse information is recovered by deploying a low-resolution (LR) and high-resolution (HR) dictionary; with the support of these dictionaries the resultant high-resolution weld microstructure image is computed. We optimize the hybrid sparsity algorithm utilizing the Sparsity-Enabled Single Value Decomposition (SE-SVD) algorithm. The calculated weld microstructure image dynamically chooses the suitable patches from the dictionary for achieving the most elegant representation among all patches for the available LR weld microstructure image. The proposed approach is resilient to noise, as it accomplishes the tasks of noise-removal and resolution enhancement at the same time. The experimental results indicate that the proposed model surpasses certain peers concerning the algorithm speed, effectiveness, and overall performance, aiding in better diagnosis of weld interface defects.

Keywords: Weld microstructure images, Resolution enhancement, Hybrid sparsity model

1 Introduction

Welding is a well-known technology for combining metal parts, and digitization of such technologies are becoming more popular due to the emergence of industry 4.0. Besides, welding technology is a widely prevalent approach for combining metals and metal parts in manufacturing and production-based firms. Tube-to-tube plate friction welding is an accessible technology that is widely deployed in many automotive firms around the world [1-2]. Figure 1 illustrates the schematic diagram of the tube-to-tube plate friction welding technology. The primary reason for automotive and other firms utilizing tube-to-tube plate friction welding is that, during the welding process, it generates less heat and a reduced amount of harmful gases than other peer welding technologies [3]. Besides, the quality of welding is a critical feature for confirming the position, distribution, and spread of the welds.

Furthermore, many industrial firms have a preference for the implementation of the tube-to-tube plate friction welding technology as the weld material never gets melted, nor it suffers from being recasted. However, weld interface defects are a common occurrence in the tube-to-tube plate friction welding process, if the welding parameters and materials involved are not correctly chosen. Also, the selection of appropriate welding parameters consumes a lot of time and resources; since it consists of several trials in finalizing the suitable welding parameters for quality welds. Figure 2 depicts the tube-to-tube plate friction welding machine.

A monitoring system for the friction stir welding (FSW) process utilizing the surface image is developed in [4]. Further, the digital cameras were utilized to acquire the weld surfaces at diverse welding conditions, and the appropriate feature is extracted from these images via the maximally stable extremal region algorithm. Then, they deploy the support vector machine algorithm for categorizing the weld images as good and bad welds [4]. The brief outline about the defects occurring in the different welding processes such as laser-beam, FSW, and arc welding for aluminum and its alloys is illustrated in [5]. In [6], the researchers devise an image processing model for identifying and categorizing the various types of FSW surface defects. Moreover, they deploy the image

*Corresponding Author: Kathiravan Srinivasan; E-mail: kathiravan.srinivasan@vit.ac.in
DOI: 10.3966/160792642020012101007

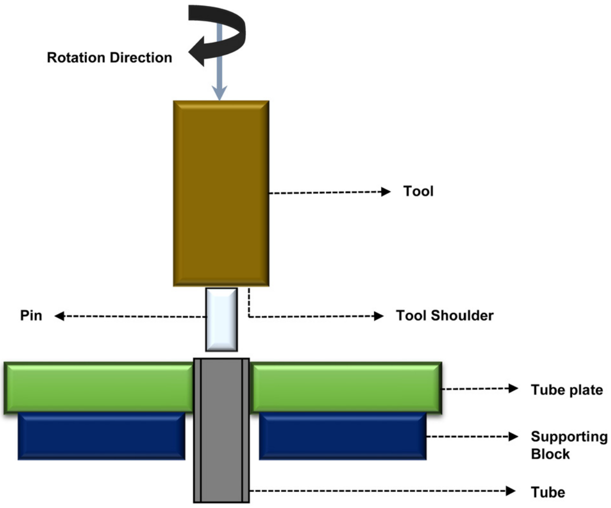

Figure 1. The schematic diagram of the tube-to-tube plate friction welding technology

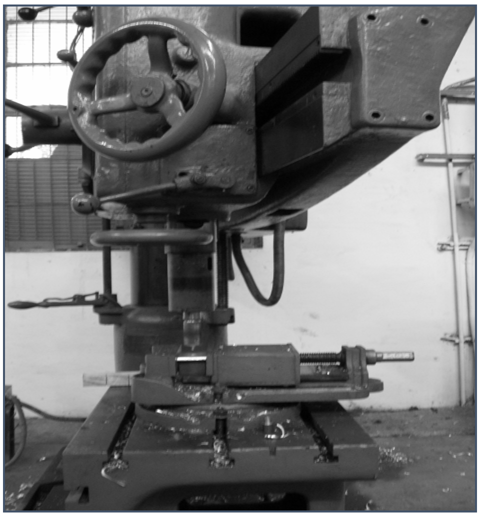

Figure 2. Tube-to-Tube plate friction welding machine

pyramid and reconstruction approaches for detecting the weld surface defects.

The researchers in [7] try to establish broad investigations about the weld surface defects using a 3D reconstructed depth map image acquired with the help of a three-dimensional optical microscope. Further, they also utilized the depth information for determining the textural features of the weld surface, such as root mean square and mean roughness. They also compared their experimental outcomes with the results from a traditional surface roughness tester equipment for validation. Wavelet transform and empirical mode decomposition are utilized for detecting and localizing the tunnel defects that occur in the FSW of the aluminum alloy [8]. In [9], the authors study the defects in FSW for two steel grades, namely DH36 and EH46. A new friction-stir welding approach for combining the aerospace-grade aluminum that can differentiate between various kinds of weld schedules for minimizing the defects in the welds [10]. The researchers in [11] deployed the friction stir welding technology for joining the AA1060 aluminum plates. Further, the weld defects were detected utilizing the damping capacity and dynamic modulus approaches. In [12], the researchers have made an effort to determine the FSW defects by utilizing the fractal theory for analyzing the signal information obtained in the course of the welding process.

Even though some researchers have tried to identify the defects in welding using computer vision and image processing, this research is still in the nascent stage and requires a lot of new automated algorithms for defects detection [14-15]. However, until now, not many researchers have attempted to improve the resolution of a degraded weld microstructure image. Therefore, in this research, we develop a new hybrid sparse model for improving the resolution of the degraded or low-resolution tube-to-tube plate friction welding microstructure images. A physically damaged or worn-out OM equipment produces a low-resolution or a degraded microstructure weld images. Determining the weld interface defects from low-resolution or degraded weld microstructure images is a challenging task for welding experts; also it might be challenging to automate the weld defect detection process, if the weld images are degraded or of low-resolution.

In this research, we deploy the hybrid sparsity model for improving the resolution of low-resolution or degraded microstructure weld images. During the course of the recovery process, the proposed model exhibits the following key characteristics, such as dynamicity, adeptness, consistency, and efficacy. The proposed hybrid sparse model outperforms the other compared algorithms concerning the peak-signal-to-noise ratio (PSNR), thereby aiding in better detection of weld interface defects.

2 Materials and Methods

2.1 Dataset Used

In this work, the dataset used was obtained using the optical microscope on the welded pieces with the Nital solution applied over it, for capturing the microstructure weld images. Before this process, the welded pieces were produced using the tube-to-tube plate friction welding machine shown in figure 2. A total of 500 weld microstructure images were used in this work; out of these, 450 images were without defects, and 50 images had weld interface defects. Figure 3. Represents the microstructure weld image without defects, and Figure 4 represents the microstructure images with weld interface defects.

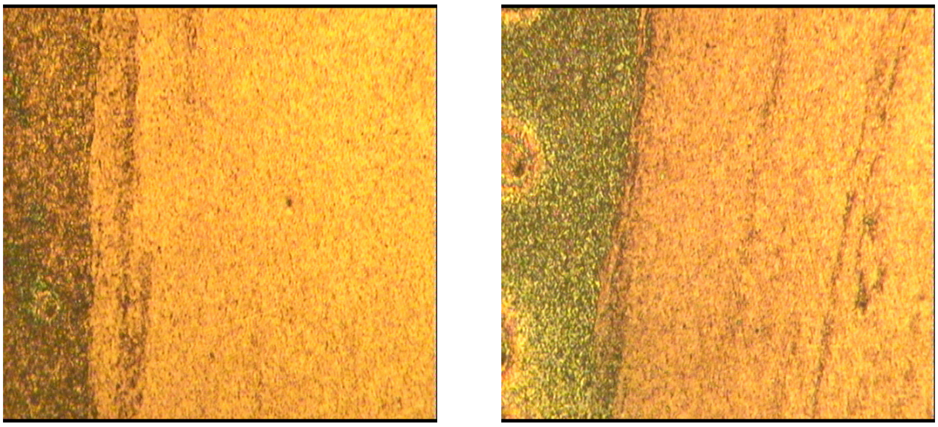

Figure 3. Fine grain weld microstructure images – good quality weld images

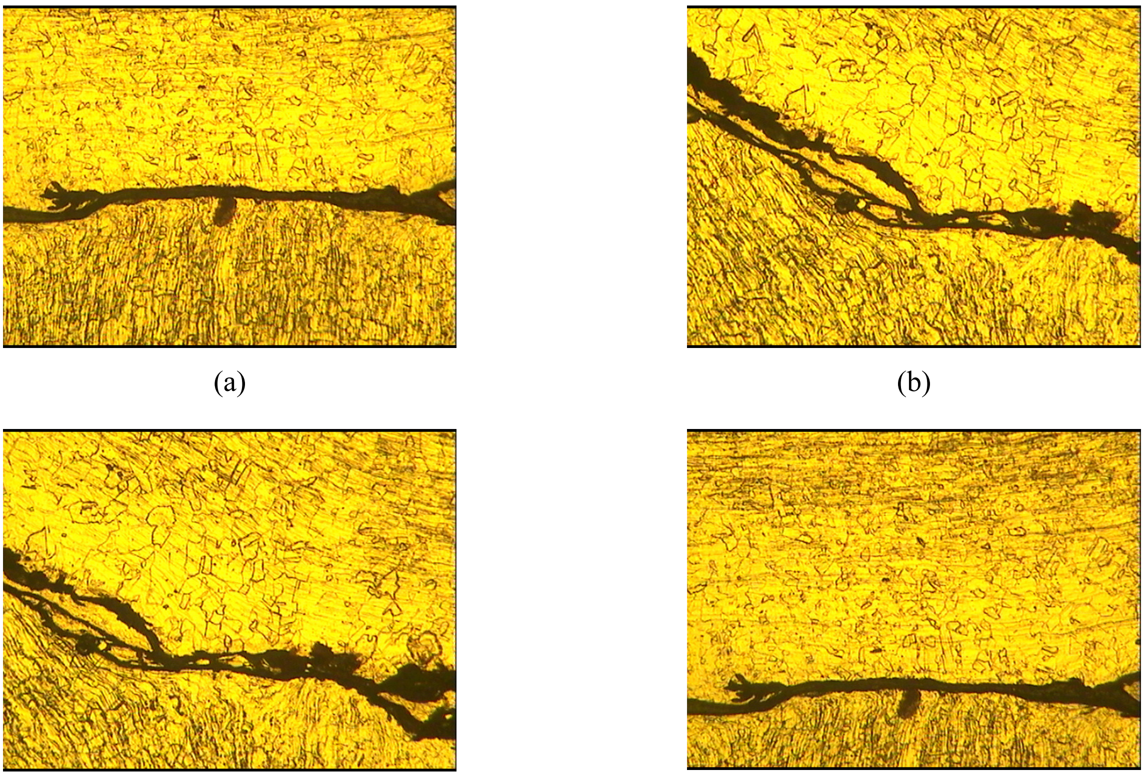

(a) (b) (c) (d)

Figure 4. Microstructure images with weld interface defects: (a) middle (b) plate (c) top (d) tube

2.2 Hybrid Sparsity Model

In this hybrid sparsity model, the signals are represented as a combination of the atom signals, in which the standard linear coefficients tend to be zero. $y \in R^M$, so the sparsity problem is illustrated as follows:

$$b = \arg\, min_b \, \| b \|_0 \;\; such\ that \, \| y - Q_b \|_2 \leq \in \quad \textbf{(1)}$$

Where b denotes the sparsity depiction of y, $\| b \|_0$ portrays the l^0 norm that specifies the total number of non-zero items, Q represents the sparsity dictionary, and $\in$ designates the error tolerance.

The sparsity dictionary Q can be illustrated as follows:

$$Q = \{q_1, q_2, q_3, \ldots\ldots, q_p\} \in R^{M \times P}, (P \geq M) \quad \textbf{(2)}$$

Where q_j indicates the sparsity atom. The proposed hybrid sparsity model establishes a sparse association amongst the high-frequency information and the low-resolution feature patches, thereby aiding in the resolution enhancement of the low-resolution or the degraded weld microstructure images. The λ represents the sparse regularization factor. The effects of the sparse regularization factor λ effects on the recovered weld microstructure image for a given input low-resolution weld microstructure image is elaborated in the later parts of this paper.

2.2.1 Sparsity Dictionary Training Process

In general, consider the training instances as $Y = \{y_1, y_2, y_3, \ldots\ldots y_s\}$

The sparsity description of Y over the sparsity dictionary Q is well-defined by the following expression:

$$B = \arg\, min_{B,W} \, \| Y - \Phi B W \|_2^2, \quad such\ that \, \| w_j \| \leq s, \quad \| b_i \|_0 \leq r, \| \Phi b_i \|_2 = 1 \quad \textbf{(3)}$$

where W signifies the sparsity description of Y, the implicit dictionary of Q is denoted by Φ; and the sparsity dictionary is indicated by B, it can be observed that B represents the sparsity coefficient of Q. Consider $V = \{Y^h, U^l\}$ to be the patch pairs of the training image, where $Y^h = \{y_1, y_2, y_3, \ldots\ldots y_m\}$, and $U^t = \{u_1, u_2, u_3, \ldots\ldots u_m\}$, a column vector is utilized for denoting the example instances $\{y_j, u_j\}$, also the term y_j indicates the high-frequency information from the high-resolution microstructure weld image feature patches and the term u_j illustrates the low-resolution microstructure weld image feature patches. Learning the sparsity dictionaries for V is one of the foremost objectives of this model and also to portray the high-resolution and low-resolution microstructure weld image feature patches in a joint frame, in a way that they share a similar sparsity description. This scenario is represented by the following equation:

$$\min_{B^h, B^l, w} [\frac{1}{M} \| Y^h - \Phi^h B^h W \|_2^2 + \frac{1}{M} \| Y^l - \Phi^l B^l W \|_2^2], \quad such\ that \, \| w_j \|_0 \leq s, \| b_i^h \|_0 \leq r, \quad \| b_i^l \|_0 \leq x, \| \Phi^h b_i^h \|_2 = 1, \quad \| \Phi^l b_i^l \|_2 = 1 \quad \textbf{(4)}$$

Where the high-frequency information of the sparsity dictionary is given by B^h, and B^l indicates the sparsity dictionary of the low-resolution microstructure weld image feature patches. Besides, M and K signifies the dimensions of the high-resolution and low-resolution microstructure weld image feature patches in the vector form. Reducing the impact of the scaling issues is another foremost goal of this model. Therefore, expression 4 is further modified and depicted using the following expression:

$$\min_{B^h, B^l, w} [\| Y - \Phi B W \|_2^2], \quad such\ that \, \| w_i \|_0 \leq r, \quad \| \Phi b_i \|_2 = 1 \quad \textbf{(5)}$$

The information concerning the values of Y, Φ, and B is represented using the following expressions:

$$Y = \begin{bmatrix} \frac{1}{\sqrt{M}} & Y^h \\ \frac{1}{\sqrt{k}} & U^t \end{bmatrix} \quad \textbf{(6)}$$

$$\Phi = \begin{bmatrix} \Phi^h & 0 \\ 0 & \Phi^t \end{bmatrix} \quad \textbf{(7)}$$

$$B = \begin{bmatrix} \frac{1}{\sqrt{M}} & B^h \\ \frac{1}{\sqrt{k}} & B^t \end{bmatrix} \quad \textbf{(8)}$$

We deploy the Sparsity-Enabled Single Value Decomposition (SE-SVD) algorithm for determining the values of expression 5. This SE-SVD algorithm is illustrated as a flow diagram in Figure 5. The essence of the orthogonal matching pursuit algorithm presented in [13] is utilized in this work.

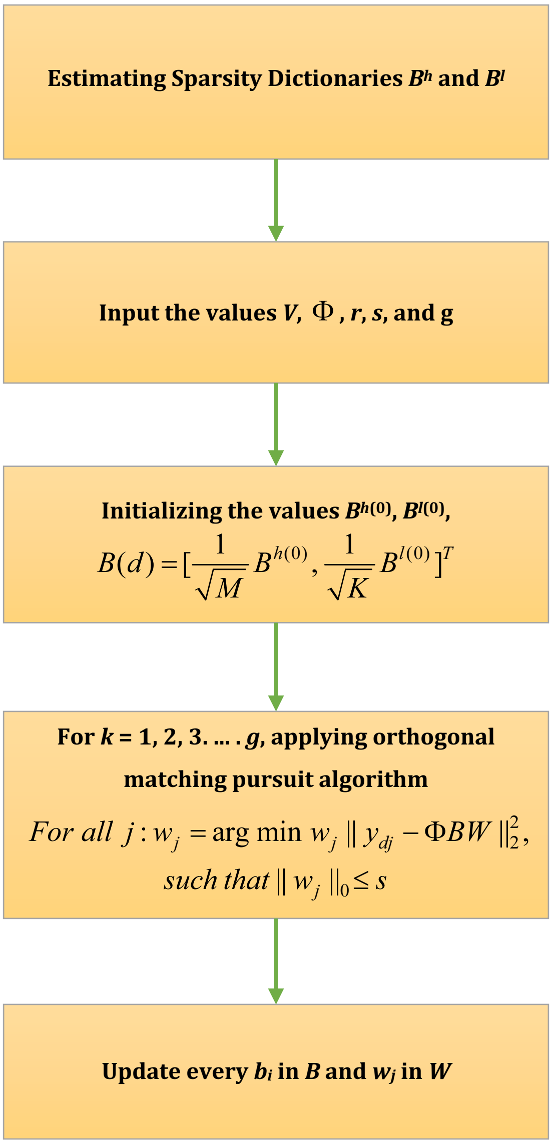

Figure 5. Flow diagram of the SE-SVD algorithm

2.2.2 Resolution Enhancement through Sparsity Dictionary

The sparsity description b is computed from the sparsity dictionary B^l by means of the low-resolution microstructure weld images feature patches denoted as u. Besides, the high-resolution microstructure weld image feature patches are computed from the sparsity dictionary B^h and the sparsity description b. The sparsity problem can be denoted by means of the following expression:

$$min \| b \|_0,$$
$$such\ that \| \Phi^l B^l b - u \|_2^2 \leq \epsilon \tag{9}$$

The expression 9 depicts a Non-deterministic Polynomial-time hard optimization problem. Then, expression 9 is aimed at all the local low-resolution microstructure weld image feature patches. Additionally, the association between the neighborhood feature patches are not considered. Further, the one-pass algorithmic approach can be deployed in order to process the microstructure weld image feature patches starting from left-to-right and also traversing top-to-bottom. Therefore the optimization problem in expression 9 is reformed as the following expression:

$$min \| b \|_1,$$
$$such\ that \| \Phi^l B^l b - u \|_2^2 \leq \epsilon_1.$$
$$\| V \Phi^h B^h b - z \|_2^2 \leq \epsilon_2 \tag{10}$$

Moreover, the vector V can be utilized for obtaining the overlapping region amidst the target high-resolution microstructure weld image feature images and the previously recuperated microstructure weld image feature patches. Besides, the value z portrays the previously recuperated overlapping microstructure weld image feature patches. As a result, the optimization problem is streamlined as following the expression:

$$\arg min_b \ \Lambda \| b \|_1 + \| \tilde{Q} b - \tilde{u} \|_2^2 \tag{11}$$

Where

$$\tilde{u} = \begin{bmatrix} \delta z \\ u \end{bmatrix}, \tilde{Q} = \begin{bmatrix} \delta V \Phi^h & B^h \\ \Phi^h & B^l \end{bmatrix} \tag{12}$$

In expression 12, the value δ handles the tradeoff amidst the input low-resolution microstructure weld image feature patches and the neighborhood compatible high-resolution microstructure weld image feature patch. The optimized value of b is computed by means of a suitable algorithm from expression 11. As a result, the high-frequency information is obtained as $y* = \Phi^h B^h b*$.

The value of primary high-resolution Y_0 by convolving the value of $y*$ and the image up-sampled from u, then the universal recuperation constraint is implemented by projecting the Y_0 values into the solution space of $U = \mathbb{Q}HY$ thereby computing the following expression:

$$Y* = \arg min_y \| Y - Y_0 \|,$$
$$such\ that\ U = \mathbb{Q}HY \tag{13}$$

Where $\mathbb{Q}$ indicates the downsampling operator, and the value H specifies the blurring filter. Then the aforementioned optimization problem is resolved utilizing the back-projection technique. The outcome of the back-projection method is denoted as $Y*$ and this value is considered as the eventual high-resolution estimate of the low-resolution microstructure weld image. The flow diagram in Figure 6 depicts this process.

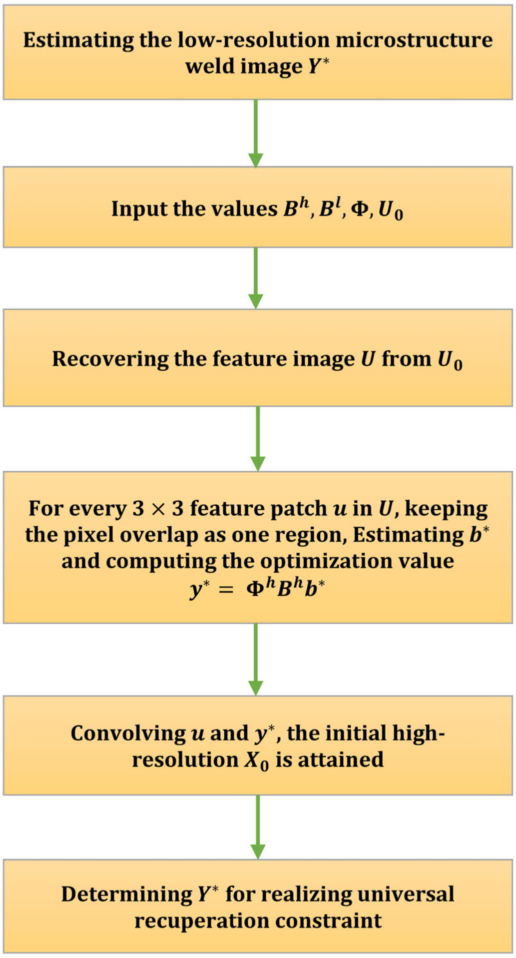

Figure 6. Flow diagram of the resolution enhancement though sparsity dictionary

2.2.3 Microstructure Weld Image Feature Patches Representation

In the proposed model, the microstructure weld image feature patches are utilized for generating the training instances. Further, the features are made up of the low-resolution weld feature patches' 1st order and 2nd order gradients. The expressions 14, 15, 16, 17 indicate the 4 filters utilized for getting the derivatives.

$$f_{11} = [-1, 0, 1] \quad \textbf{(14)}$$

$$f_{12} = f_{11}^T \quad \textbf{(15)}$$

$$f_{21} = [1, 0, -2, 0, 1] \quad \textbf{(16)}$$

$$f_{22} = f_{21}^T \quad \textbf{(17)}$$

The features are made up of the high-frequency information taken from the high-resolution microstructure weld patches of the image. As a result, each training instance gets a vector description, and this is made up of the low-resolution image patches' 4 gradient features and high-frequency information acquired from the high-resolution microstructure weld patches of the image. Figure 7 depicts the aforementioned scheme.

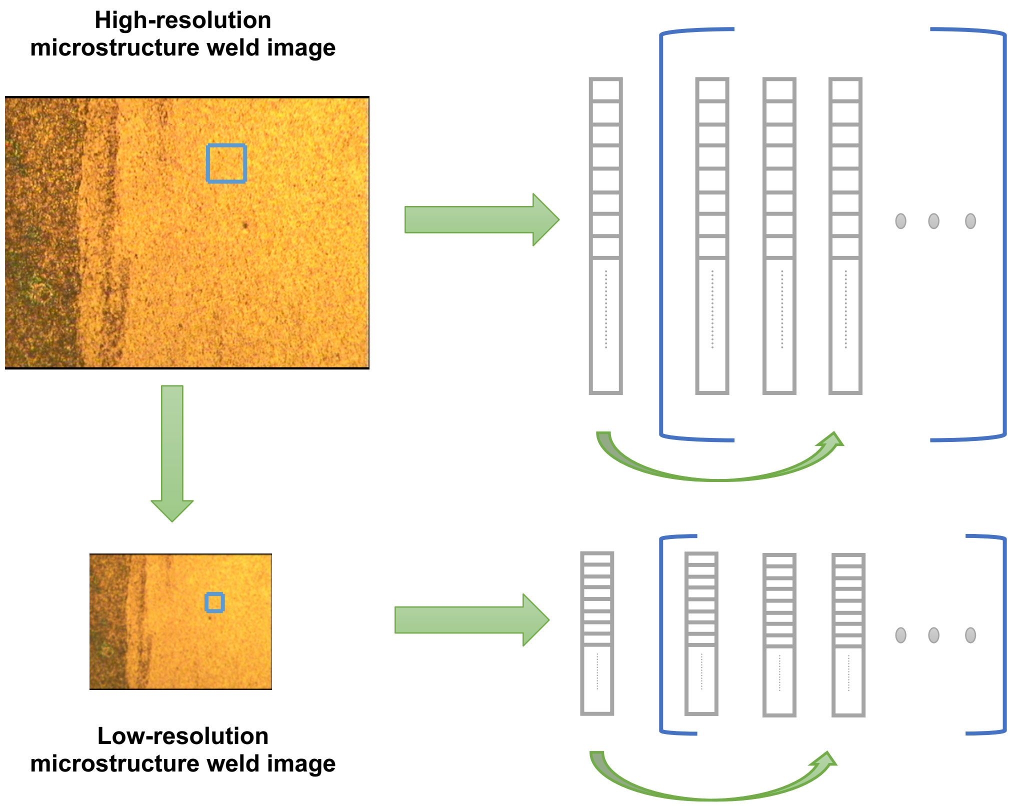

Figure 7. The training instance has two components namely the high-frequency patch from the high-resolution microstructure weld image and 1st and 2nd order gradient features of the low-resolution microstructure weld image

4 Experimental Results

In this section, we compare the outcomes of the various prevailing approaches such as bi-cubic interpolation, k-nearest neighbors' algorithm, Locally Linear Embedding, Non-local means algorithm with the proposed hybrid sparsity model. Besides, we also focus on the various factors like noise immunity and the size of the sparsity dictionary that has a significant impact on the performance of the proposed hybrid sparsity model. In this research, the motivation is to apply the proposed hybrid sparsity model on the illuminance channel of the microstructure weld images. The primary reason for the aforementioned strategy is due to the human visual senses having a higher sensitivity towards the variations in the luminance. Besides, in the upcoming portions, we also present the visual and qualitative outcomes of the aforementioned methods. Further, for the qualitative assessment, we utilize the peak-signal-to-noise (PSNR) measure that is defined as follows:

$$PSNR = 20\log_{10}\left(\frac{MAX_f}{\sqrt{Mean\ Square\ Error}}\right) \quad \textbf{(18)}$$

Where, MAX_f indicates the maximum value of the signal from the original right microstructure weld image.

The proposed hybrid sparsity model is utilized for enhancing the resolution of the low-resolution or degraded micro-structure weld images. The training scheme of both the high-resolution and low-resolution sparsity dictionaries' is performed using 75,000 patch pairs. Besides, these patch pairs were gathered from the input microstructure weld image dataset. Furthermore, they are also deployed as training instances for the proposed hybrid sparsity model. A quick pre-processing is done over these microstructure weld images. The pre-processing phase includes the removal of unnecessary texture areas and also ignoring the smooth surfaces. In our experiments, we have chosen the size of the sparsity dictionaries' to be 1024. The reason for choosing this value for maintaining an equilibrium amidst the computational time and the microstructure weld image quality. The noise level in the input microstructure weld image plays a significant role in choosing the value of the regularization parameter Λ The Λ value is chosen as 0.01 for the microstructure weld images with less noise. Besides, this value of the regularization parameter yields rational outcomes.

In this research, the gathered microstructure weld images are primarily downsampled by a factor with the value 1/3 for the next stage of processing. Furthermore, the downsampled microstructure weld images are then upsampled by a factor with value 3 by utilizing the proposed hybrid sparsity model, and other methods like bi-cubic interpolation, k-nearest neighbors' algorithm, Locally Linear Embedding, Non-local means algorithm are also deployed for enhancing the resolution of such images. While designing this proposed hybrid sparsity model, we have assumed a 3×3 low-resolution microstructure weld image patches. Besides, these patches are considered to possess the overlapping of one-pixel with its constituent adjacent patches. Subsequently, we also presume that the 9×9 high-resolution microstructure weld image patches possess an overlapping three-pixels with its adjacent regions. Besides, the low-resolution microstructure weld images are upsampled with a value 2. Another significant point is that the 1st order and the 2nd order gradient features are obtained from the upsampled version of the low-resolution microstructure weld images. It can be observed that the size of the upsampled low-resolution microstructure weld image is 6×6.

Table 1 depicts the comparison of the PSNR of the proposed hybrid sparsity model with other methods. We can clearly observe that the graphical representation in Figure 8 gives a clear distinction of the superior performance of the proposed hybrid sparsity model than the other approaches. Figures 9, 10, 11 illustrates the visual outcomes of the experiments conducted over the microstructure weld images for the proposed hybrid sparsity model in comparison with algorithms like bi-cubic interpolation, k-nearest neighbors' algorithm, Locally Linear Embedding, Non-local means. Besides, from these figures, it is evident that the proposed hybrid sparsity model produces outcomes with superior visual appearance. Also, the proposed model outperforms the other compared models concerning the computational swiftness.

Table 1. Comparison of the PSNR (dB) of the proposed hybrid sparsity model with other methods

Weld Microstructure Images\Methods	Bi cubic interpolation	K-nearest neighbors	Locally Linear Embedding	Non-local means	Hybrid sparsity model
Image 1	23.89	25.66	27.32	28.52	29.86
Image 2	21.16	22.98	24.69	26.32	29.79
Image 3	25.28	25.87	26.75	26.98	29.02

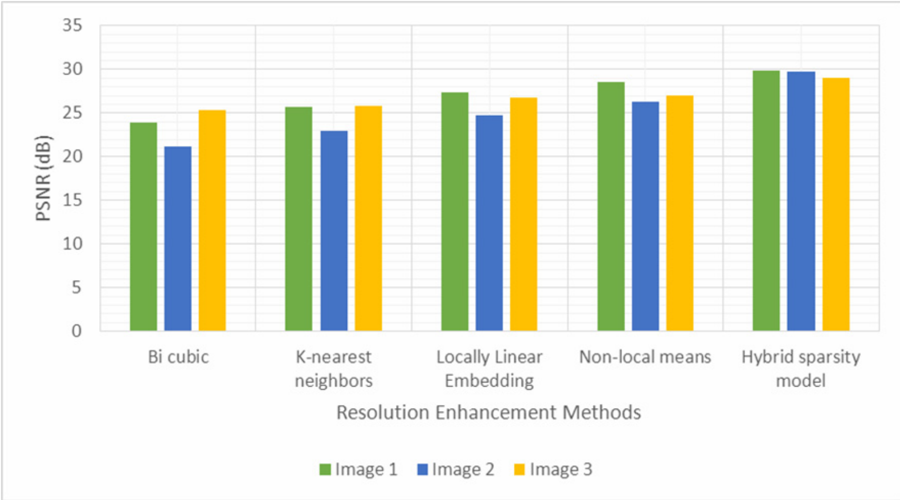

Figure 8. Graphical Representation of PSNR (dB) – Resolution Enhancement Methods

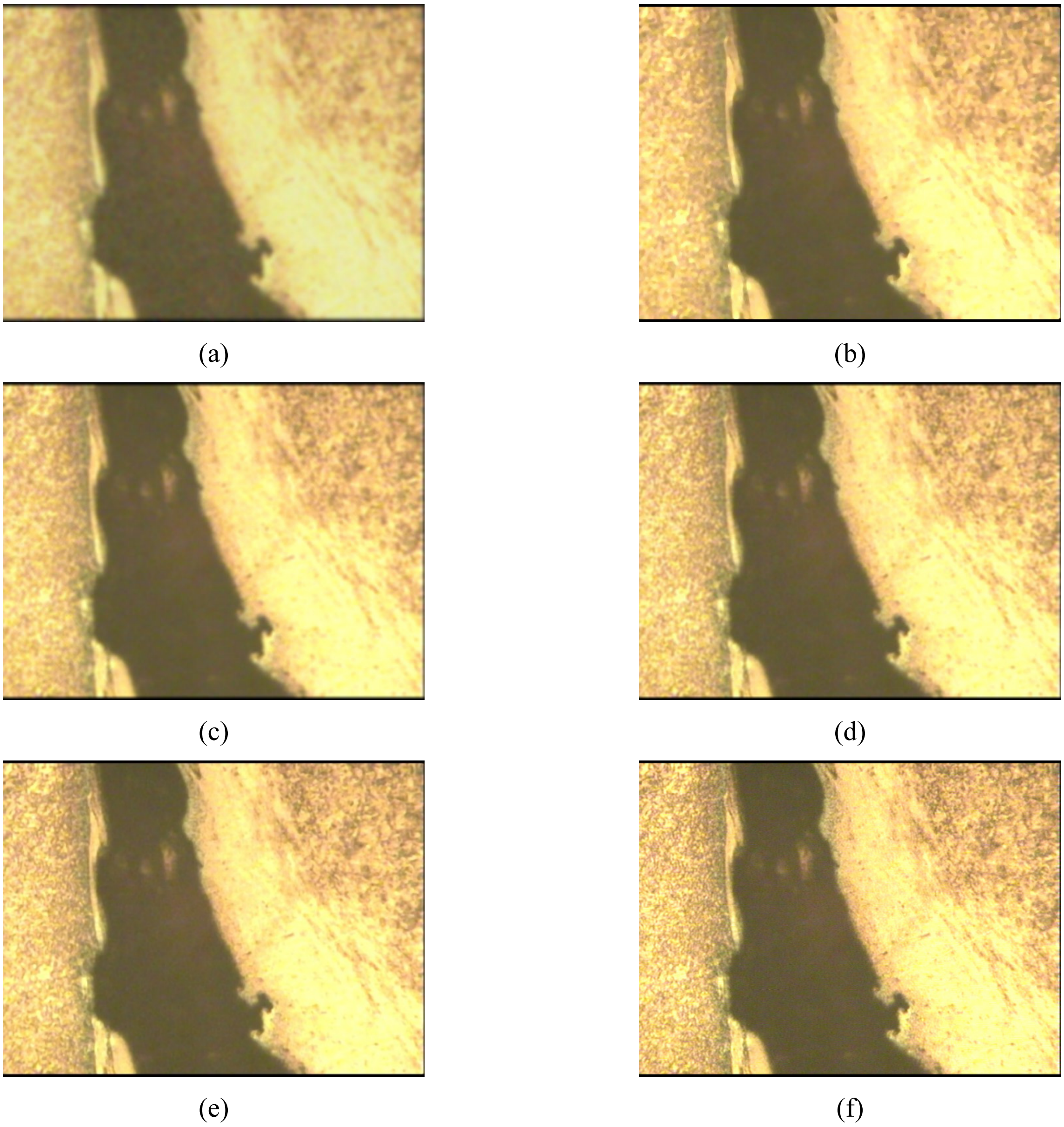

Figure 9. Image 1: (a) Low-resolution microstructure weld image; Resolution Enhancement Methods: (a) Bicubic interpolation, (b) K-nearest neighbors, (c) Locally Linear Embedding, (d) Non-local means, (e) Hybrid sparsity model

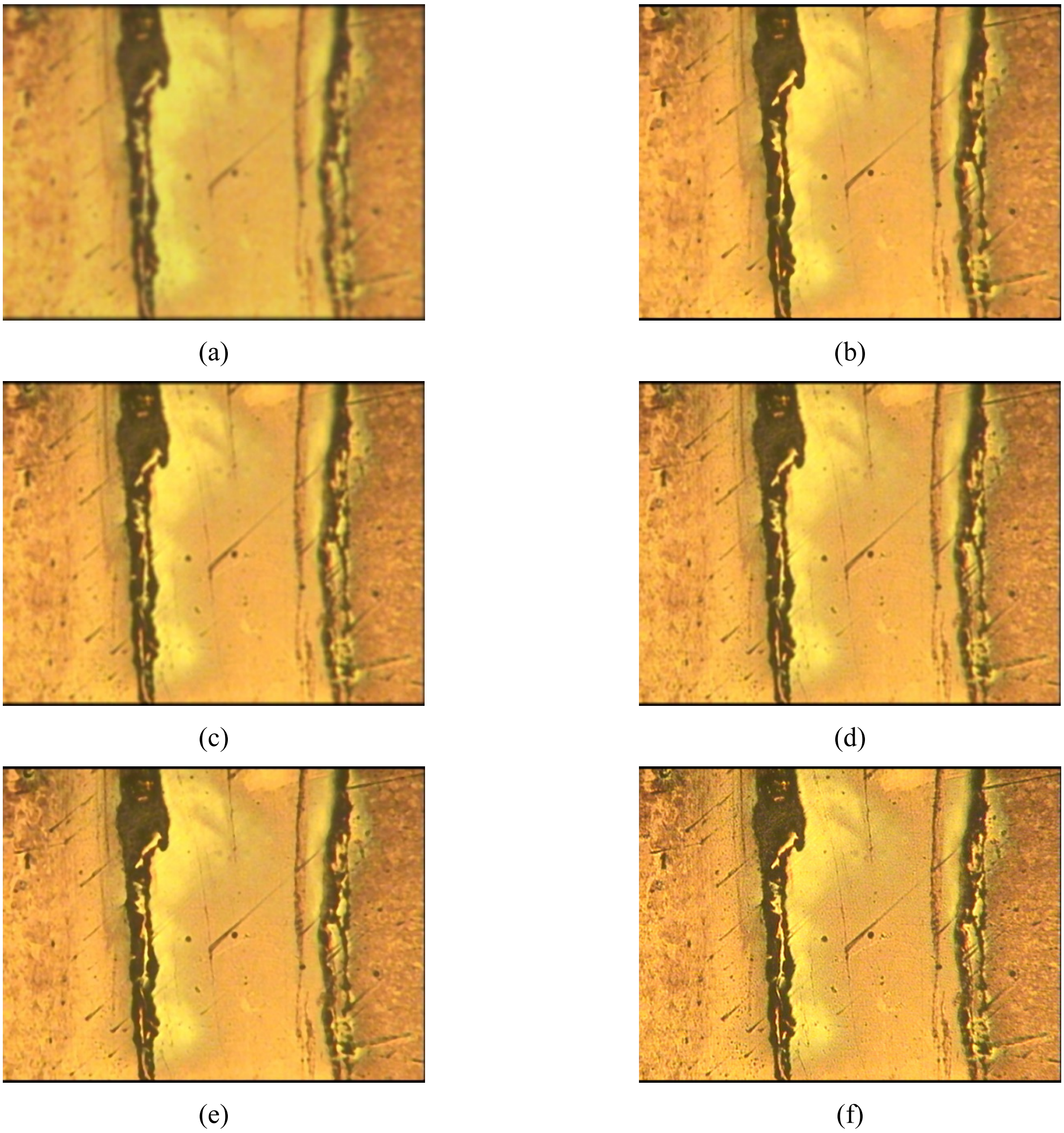

Figure 10. Image 2: (a) Low-resolution microstructure weld image; Resolution Enhancement Methods: (a) Bi cubic interpolation, (b) K-nearest neighbors, (c) Locally Linear Embedding, (d) Non-local means, (e) Hybrid sparsity model

4.1 Size of Sparsity Dictionary and its Effect

We now focus on the size of the sparsity dictionary for the recuperating the low-resolution microstructure weld images. It is well depicted in Figure 12 that the computational time-period (in seconds) on the low-resolution microstructure weld image for various sparsity dictionary sizes of 256, 512, 1024, 2048 have been implemented. In most of our experiments, we have chosen the size of the sparsity dictionary as 1024. Usually, we can observe that larger the size of the sparsity dictionary, superior will be its performance, as well as it gives accurate estimated outcomes. Further, with the increasing size of the sparsity dictionary, the computational expenditure gets higher. Also, a closer observation gives the view that the distinct sizes of the sparsity dictionaries ranging from 256 till 2048, produces the experimental outcomes that are not so visually divergent. Besides, the microstructure weld image sample patches for distinct sparsity dictionary sizes appear to be identical in terms of visual perception. Also, the critical point is the artifacts appearing after the reconstruction process starts fading down when the sparsity dictionary sizes become larger and larger. Although the total number of computations is directionally proportional to the size of the sparsity dictionary, they produce better results. Besides, the larger the size of the sparsity dictionary, the higher will be the number of computations. Further, through our experiments, we found that the sparsity dictionary size having a value 1024 generates superior outcomes, and also it is equally fast in terms of overall computations.

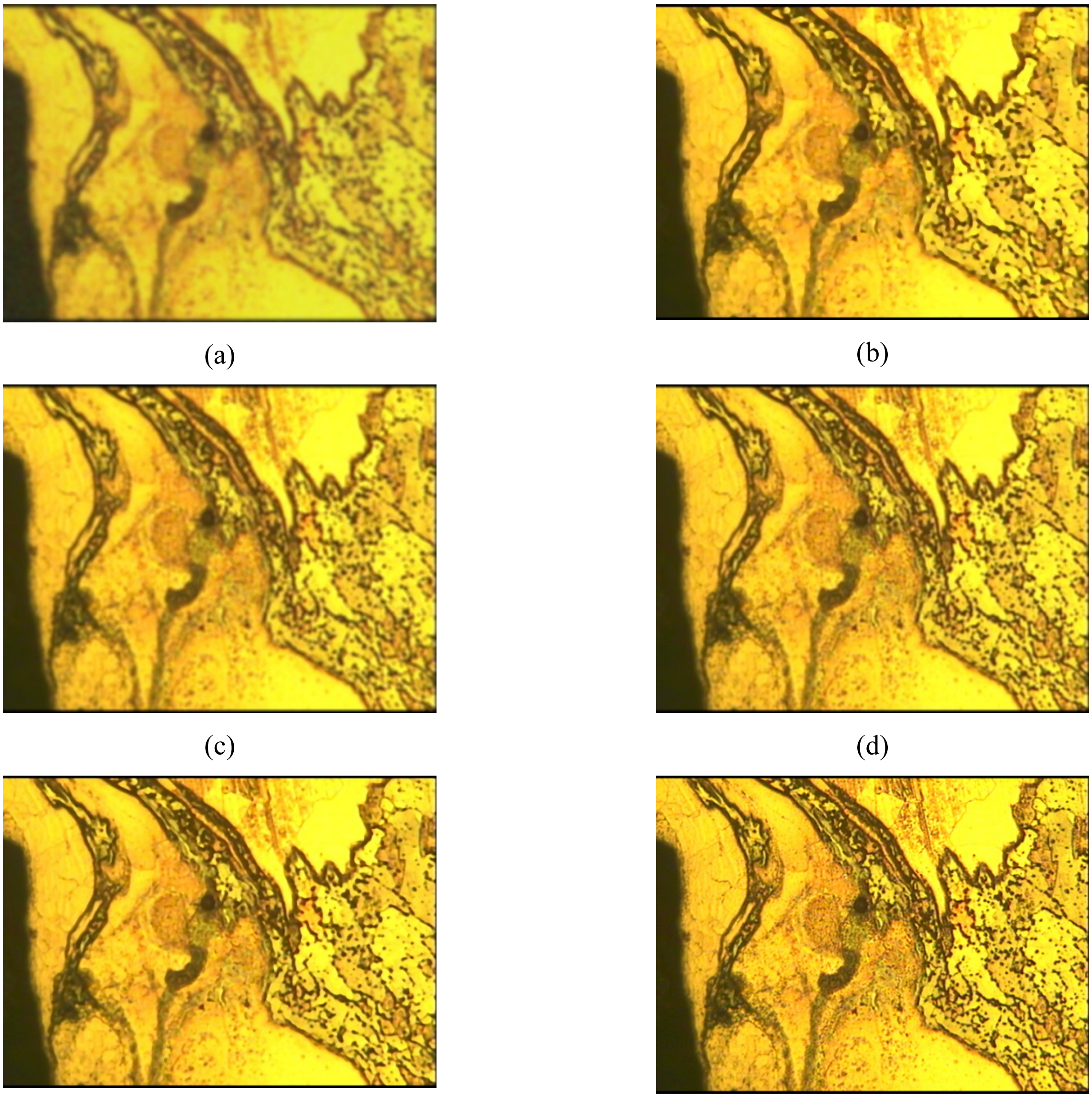

(a) (b) (c) (d) (e) (f)

Figure 11. Image 3: (a) Low-resolution microstructure weld image; Resolution Enhancement Methods: (a) Bi cubic interpolation, (b) K-nearest neighbors, (c) Locally Linear Embedding, (d) Non-local means, (e) Hybrid sparsity model

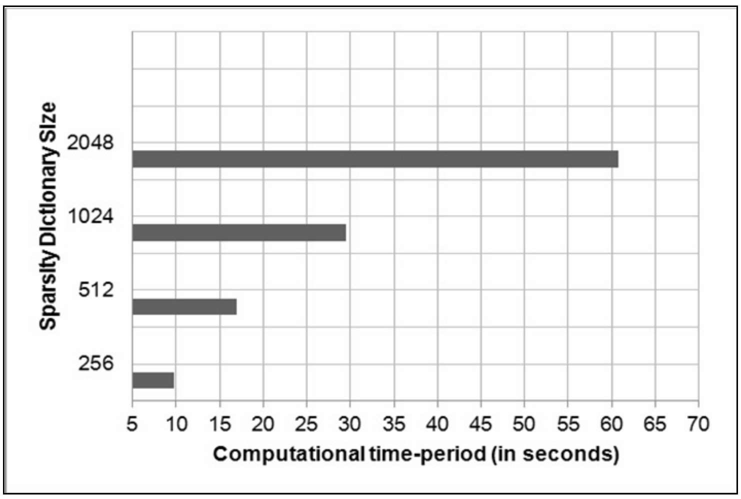

Figure 12. Computational time-period (seconds) for the low-resolution microstructure weld images having the sparsity dictionary size with values 256, 512, 1024, and 2048

4.2 Noise Immunity and Regularization Parameter Λ Effects

From the previous Figures 9, 10, and 11, we can understand that the proposed hybrid sparsity model is highly robust to noise and also performs well when the input low-resolution microstructure weld image is corrupted by noise. During the experiments, the value of the regularization parameter Λ is chosen based on the presence and availability of noise or unwanted information in the input low-resolution microstructure weld images. Also, it is understood that for noisy images, higher values of the regularization parameter Λ produces excellent results concerning the visual perception. Besides, increasing values of the regularization parameter Λ might also generate smooth texture regions in the resultant microstructure weld images.

5 Conclusion

In this research, we propose an approach, namely the hybrid sparsity model for enhancing the resolution of the low-resolution microstructure weld images. Further, in this method, the sparsity association amidst the high-resolution and the low-resolution microstructure weld image feature patches is articulated. Besides, this model also does the matching and optimization in a parallel way. The proposed hybrid sparsity model performs stably, and it is also effective. Besides, it also necessitates lesser instances for generating a high-resolution microstructure weld image. The proposed hybrid sparsity model performs exceedingly well concerning computational speed, quality outcomes, and noise immunity. Finally, it exhibits a more exceptional performance than the other compared approaches. The proposed hybrid sparsity model thereby helps in improved weld interface defects diagnosis. The future works shall cogitate, adapting probability integrated machine learning approaches [16-18]. Assuming uncertainties for applications in complex welding processes and comparing the analysis to that conducted in the present study.

References

[1] M. Stütz, R. Buzolin, F. Pixner, C. Poletti, N. Enzinger, Microstructure Development of Molybdenum During Rotary Friction Welding, *Materials Characterization*, Vol. 151, pp. 506-518, May, 2019.

[2] M. Chludzinski, R. E. dos Santos, D. R. Pissanti, F. C. Kroeff, F. Mattei, G. Dalpiaz, M. T. Piza Paes, Full-scale Friction Welding System for Pipeline Steels, *Journal of Materials Research and Technology*, Vol. 8, No. 2, pp. 1773-1780, April, 2019.

[3] S. S Kumaran, A. D Das, An Examination of Seamless Ferritic Tube and Austenitic Alloy Tube Plate Joining by Friction Welding Process, *Materials Today: Proceedings*, Vol. 5, No. 2, Part 2, pp. 8539-8546, January, 2018.

[4] S. Sudhagar, M. Sakthivel, P. Ganeshkumar, Monitoring of Friction Stir Welding Based on Vision System Coupled with Machine Learning Algorithm, *Measurement*, Vol. 144, pp. 135-143, October, 2019.

[5] P. Kah, R. Rajan, J. Martikainen, R. Suoranta, Investigation of Weld Defects in Friction-stir Welding and Fusion Welding of Aluminium Alloys, *International Journal of Mechanical and Materials Engineering*, Vol. 10, No. 26, pp. 1-10, December, 2015.

[6] R. Ranjan, A. R. Khan, C. Parikh, R. Jain, R. P. Mahto, S. Pal, S. K. Pal, D. Chakravarty, Classification and Identification of Surface Defects in Friction Stir Welding: An Image Processing Approach, *Journal of Manufacturing Processes*, Vol. 22, pp. 237-253, April, 2016.

[7] C. Parikh, R. Ranjan, A. R. Khan, R. Jain, R. P. Mahto, D. Chakravarty, S. Pal, S. K. Pal, Volumetric Defect Analysis in Friction Stir Welding Based on Three Dimensional Reconstructed Images, *Journal of Manufacturing Processes*, Vol. 29, pp. 96-112, October, 2017.

[8] J. Rabi, T. Balusamy, R. Raj Jawahar, Analysis of Vibration Signal Responses on pre Induced Tunnel Defects in Friction Stir Welding Using Wavelet Transform and Empirical Mode Decomposition, *Defence Technology*, May, 2019, https://doi.org/10.1016/j.dt.2019.05.014.

[9] M. Al-Moussawi, A. J. Smith, Defects in Friction Stir Welding of Steel, *Metallography, Microstructure, and Analysis*, Vol. 7, No. 2, pp 194-202, April, 2018.

[10] M. A. Wahab, M. W. Dewan, D. J. Huggett, A. M. Okeil, T. W. Liao, A. C. Nunes, Challenges in the Detection of Weld-defects in Friction-stir-welding (FSW), *Advances in Materials and Processing Technologies*, Vol. 5, No. 2, pp. 258-278, February, 2019.

[11] W. S. AbuShanab, E. B. Moustafa, Detection of Friction Stir Welding Defects of AA1060 Aluminum Alloy Using Specific Damping Capacity. *Materials*, Vol. 11, No. 12, 2437, pp. 1-14, November, 2018.

[12] B. Das, S. Pal, S. Bag, Defect Detection in Friction Stir Welding Process Using Signal Information and Fractal Theory, *Procedia Engineering*, Vol. 144, pp. 172-178, May, 2016.

[13] T. T. Cai, L. Wang, Orthogonal Matching Pursuit for Sparse Signal Recovery with Noise, *IEEE Transactions on Information Theory*, Vol. 57, No. 7, pp. 4680-4688, July, 2011.

[14] E. Yahaghi, M. Hosseini-Ashrafi, Enhanced Defect Detection in Radiography Images of Welded Objects, *Nondestructive Testing and Evaluation*, Vol. 34, No.1, pp. 13-22, November, 2019.

[15] H. Zhu, W. Ge, Z. Liu, Deep Learning-based Classification of Weld Surface Defects, *Applied Sciences*, Vol. 9, No. 16, 3312, August, 2019.

[16] W. Li, S. Chen, X. Peng, M. Xiao, L. Gao, A. Garg, N. Bao, A Comprehensive Approach for the Clustering of Similar-

Performance Cells for the Design of a Lithium-Ion Battery Module for Electric Vehicles, *Engineering*, Vol. 5, No. 4, pp. 795-802, July, 2019.

[17] X. Mo, X. Hu, J. Tang, H. Tian, A Comprehensive Investigation on Thermal Management of Large-capacity Pouch Cell Using Micro Heat Pipe Array, *International Journal of Energy Research*, Vol. 43, No. 13, pp. 7444-7458, August, 2019.

[18] D. Jiang, K. Wu, D. Chen, G. Tu, T. Zhou, A. Garg, L. Gao, A Probability and Integrated Learning Based Classification Algorithm for High-level Human Emotion Recognition Problems, *Measurement*, Vol. 150, 107049, January, 2020.

Biographies

Kathiravan Srinivasan received his B.E. (ECE), M.E., (CS) and Ph.D., (ICE) from Anna University Chennai, India. He is presently working as an Associate Professor in the School of Information Technology and Engineering at Vellore Institute of Technology (VIT), Vellore, India. His research interests include Machine Learning, Image Processing, Communication Systems & Networks, Multimedia, and Vehicular Networks.

N Deepa is working as Assistant Professor (Senior) in the School of Information Technology and Engineering, Vellore Institute of Technology (VIT), Vellore, India. She has pursued her M.E. in CSE and her Doctoral degree in Anna University and VIT, Vellore, respectively. Her areas of interest are Machine Learning, Soft computing, Data mining, Artificial Intelligence, Predictive Analytics.

Durai Raj Vincent P M received his B.E. and M.E. from Anna University, Chennai, India. He received his Ph.D., from VIT University Vellore. He is presently working as an Associate Professor in the School of Information Technology and Engineering at Vellore Institute of Technology (VIT), India. His current research interest includes Security, Machine Learning, and Data Analytics.

Senthil Kumaran S is presently working as the Associate Professor in the School of Mechanical Engineering, Vellore Institute of Technology (VIT), Vellore, India. He completed his Ph.D. from the Department of Metallurgical and Materials Engineering, National Institute of Technology Tiruchirappalli. His current research interests include microstructure, testing, and evaluation, materials processing and characterization, welding, optimization.